director in each bubble near the air interface is vertical (9). Similarly, the bottom portion of each bubble is in contact with the isotropic phase, where measurements indicate that the director is anchored at an angle $\theta_{NI} = 63.5° \pm 0.6°$ from the vertical (14–16).

This configuration of directors is illustrated in Fig. 3. The two-headed arrows on each vertical dotted line represent the directors for the top, the bulk, and the bottom of a given bubble. After coalescence, the application of the geodesic rule for this configuration of directors is consistent with the emergence of a horizontal string, as indicated by the bold solid line. This model for string formation accounts for the observed absence of strings terminating at the interfaces. Strings certainly do not pass through the top, because the director orientation is constant everywhere. Although the director at the bottom sites can have some variation, no string can pass through the bottom faces. This limitation is because the entire bottom face (including the links) is supposed to represent the N-I interface where the director has fixed anchoring. For the bottom face, the geodesic rule is applied with this additional restriction on the director orientation. A little thought then reveals that a strength 1/2 line defect cannot pass through the bottom face of the lattice. Because in our experiment we only see the two-dimensional projected length of the string, we estimated the horizontally projected average length of the strings per bubble of unit size. We generated 50,000 random configurations of directors, consistent with the boundary conditions, and computed the corresponding value of n_s to be 1.564 ± 0.006 (17).

This model is in fair agreement with our observations—it accounts for the formation of strings that do not terminate at the upper and lower interfaces and for the magnitude of the string length. There are two primary deficiencies. First, the model predicts two layers of strings, upper and lower. We have no clear evidence for more than a single layer; we do not clearly observe one string passing beneath another without contact. Second, the predicted string length is about twice as great as that observed. This quantitative discrepancy may be partially explained by string interactions in the seconds that pass between our last clear image of bubbles and our first clear image of strings (see Fig. 2, C and D), but a model that more clearly accounts for a single layer would also reduce the discrepancy.

We can account well for the observed string length if we assume that our measurements are sensitive primarily to strings at the air-nematic interface. It is plausible that the coalescence of two nematic bubbles forms horizontal strings that are in effect squeezed toward the interfaces; we anticipate that the free energy of strings at the air-nematic interface is significantly lower than that for bulk strings, so that the formation of a mat of strings at this interface is favored. The disadvantage of this approach is that we did not clearly observe structures that would correspond to a string descending from the surface toward the N-I interface. We speculate that intercommutation (3) may have disconnected the strings leading down from the surface mat during the several seconds that passed between our last clear image of bubbles (Fig. 2C) and our first clear image of strings (Fig. 2D). In any event, we reanalyzed the simulation described earlier to estimate the horizontal length of just the strings in the top half of Fig. 3. This reconsideration yields $n_s = 0.636 \pm 0.004$—in excellent agreement with our measured value (18).

REFERENCES AND NOTES

1. T. W. B. Kibble, *J. Phys. A Gen. Phys.* **9**, 1387 (1976).
2. W. H. Zurek, *Nature* **317**, 505 (1985).
3. I. Chuang, R. Durrer, N. Turok, B. Yurke, *Science* **251**, 1336 (1991).
4. I. Chuang, N. Turok, B. Yurke, *Phys. Rev. Lett.* **66**, 2472 (1991).
5. P. C. Hendry, N. S. Lawson, R. A. M. Lee, P. V. E. McClintock, C. D. H. Williams, *Physica B*, in press.
6. P. G. de Gennes, *The Physics of Liquid Crystals* (Clarendon, Oxford, 1974).
7. Technically, the resultant space S^2/Z_2 is called the projective plane RP^2.
8. N. D. Mermin, *Rev. Mod. Phys.* **51**, 591 (1979).
9. Y. Bouligand, in *Les Houches Session XXXV, Physics of Defects*, R. Balian, Ed. (North-Holland, Dordrecht, Netherlands, 1981).
10. M. Kleman, *Points, Lines and Walls in Liquid Crystals, Magnetic Systems and Various Ordered Media* (Wiley, Chichester, 1983).
11. S. Chandrasekhar and G. S. Ranganath, *Adv. Phys.* **35**, 507 (1986).
12. The assumption of the least variation of θ used above is called the geodesic rule. The rule is a plausible consequence of minimizing the gradient energy associated with the spatial variation of θ.
13. T. Vachaspati, *Phys. Rev. D* **44**, 3723 (1991).
14. S. Faetti and V. Palleschi, *Phys. Rev. A* **30**, 3241 (1984).
15. A curious implication of the N-I boundary conditions is that an isolated nematic bubble should contain a monopole topological defect. This condition may not apply in sufficiently small bubbles [the so-called thick wall bubbles; for example, see (*16*)]; inside such bubbles the magnitude of the director is smaller than the value appropriate for the nematic phase (*16*).
16. A. M. Srivastava, *Phys. Rev. D* **45**, R3304 (1992); *ibid.* **46**, 1353 (1992).
17. We also checked the dependence of n_s on the anchoring angle θ_{NI} of the director at the N-I interface. For $\theta_{NI} = 0.0$, n_s is found to have a smallest value equal to 1.264. The number of strings per bubble increases monotonically with θ_{NI}, from $n_s = 1.34$ for $\theta_{NI} \simeq 30°$ to a maximum value of 1.628 for $\theta_{NI} = \pi/2$. This dependence of n_s on θ_{NI} is easy to understand because with increasing θ_{NI}, the allowed values for the director form a larger and larger set (which leads to a larger n_s for a cubic lattice), with the largest set attained at $\theta_{NI} = \pi/2$.

18. We thank M. Hindmarsh, P. Palffy-Muhoray, G. Ranganath, C. Rosenzweig, and B. Yurke for discussions and E. Lipson for making these experiments possible. Supported by U.S. Department of Energy (DOE) grant DE-FG02-85ER40231 (to M.J.B.) and by National Science Foundation grant PHY89-04035 and DOE contract DE-AC02-83ER40105 at the University of Minnesota (to A.M.S.).

13 October 1993; accepted 3 December 1993

Laser-Based Analysis of Carbon Isotope Ratios

D. E. Murnick* and B. J. Peer†

A laser technique for analysis of carbon-13 : carbon-12 ratios with the specificity of laser resonance spectroscopy and the sensitivity and accuracy typical of isotope ratio mass spectrometers is reported. The technique is based on laser optogalvanic effect spectroscopy, in which an electrical (galvanic) signal is detected in response to the optical stimulation of a resonance transition in a gas discharge species. Carbon dioxide molecular gas lasers are used, with the probed transitions being identical to the lasing transitions. Measurements for carbon dioxide samples with 100-second averaging times yield isotopic ratios with a precision of better than 10 parts per million.

Carbon isotopic analysis is an important tool in geology (1), environmental science (2), biology (3), and medicine (4). In geological studies, such as the sedimentation of carbonates, or in atmospheric studies, such as polar ice core and oceanic isotope measurements, it is the $^{13}CO_2 : ^{12}CO_2$ ratio that is of primary importance in the determination of the cycle of CO_2 production and absorption throughout history. In biological and medical studies, analysis of isotopic carbon ratios makes possible the study of metabolic pathways in living systems. Presently, either the radioactive tracer ^{14}C or stable ^{13}C is used for such analysis. The use of ^{13}C as a tracer for diagnostic purposes is a rapidly growing field (5). The use of stable ^{13}C rather than the radioactive isotope ^{14}C obviates potential harmful radiation effects and eliminates time constraints and the problem of radioactive waste disposal.

Department of Physics, Rutgers University, Newark, NJ 07102, USA.

*To whom correspondence should be addressed.
†Present address: Department of Geology and Planetary Science, University of Pittsburgh, Pittsburgh, PA 15260, USA.

At present, stable isotope analysis of carbon is carried out with sensitive but expensive and sophisticated mass spectrometers, which are capable of determining isotope ratio changes as small as one part in 10,000. Conventionally, results are expressed in relative differential units δ, with respect to a standard (*6*). Normally, CO_2, the oxidation product of carbon-containing compounds, is analyzed in the mass spectrometer, which measures the ratio of mass 45 to mass 44 (*7*). High-quality vacuums and low impurity levels, especially of water vapor, must be scrupulously maintained. The mass spectrometer measures mass so, for example, $^{12}COOH$ mimics $^{13}CO_2$, as does $^{12}C^{16}O^{17}O$.

Laser methods of isotopic analysis based on the isotope shift in spectral lines have been reported. Transitions at specific wavelengths are unique signatures for a given species. Typically, a continuously tunable laser is used whose frequency range spans spectral features arising from transitions involving the isotopes of interest. For atomic species, isotopic analysis is complicated by hyperfine structure (*8*) and relatively small spectral shifts for most species (*9*). For light isotopes, resonance transitions are most often in the ultraviolet spectral region, where fewer tunable lasers are available. Line narrowing techniques, such as the use of atomic beams or laser saturation spectroscopy, are also often required to achieve the desired spectral resolution.

For molecular species, the isotopic shifts in vibration-rotation spectra, often in the infrared spectral region, can serve as the basis of isotopic analysis (*10*). Typically, ground-state absorption spectroscopy is used; however, very long absorption paths are necessary to achieve sufficient quantitative measures of weak spectral features. Laser techniques for isotopic ratio analysis have not had widespread use to date because of a lack of sufficient sensitivity and of suitable tunable lasers.

We report a laser technique for isotopic analysis of $^{13}CO_2 : {}^{12}CO_2$ that has both the specificity of laser resonance spectroscopy and the sensitivity of a mass spectrometer. The technique makes use of laser optogalvanic effect spectroscopy (*11*). The optogalvanic effect signal is an electrical (galvanic) signal detected in response to optical stimulation of a resonance transition in an electrical discharge species. In a dc discharge, resistivity can be monitored; in an ac discharge, any quantity related to discharge impedance can be used. The output voltage of a radio-frequency (rf) oscillator that provides power to a tuned circuit was found to be effective (*12*).

Unlike laser absorption or fluorescence measurements, no optical measurement is required, eliminating all collection and dispersion optics and light transducers. Any optical background noise that might obscure the desired signal is eliminated. Unlike mass spectroscopic ion current measurements, the optogalvanic effect resonance signal is essentially unique to the species ($^{13}CO_2$ or $^{12}CO_2$) being investigated, so purification or concentration of the sample is usually not required.

A CO_2 molecular gas laser was used, and the resonance transition being probed was identical to the lasing transition (Fig. 1). The CO_2 laser first used was a grating tunable laser operating with a mixture (approximately 1 : 1) of $^{13}CO_2$ and $^{12}CO_2$ (*13*). Many different vibration-rotation transitions can be made to lase in CO_2 (*14*). Wavelength shifts resulting from isotopic substitutions tend to be large and have been studied for several years (*15*). Almost any of the laser transitions unambiguously associated with one or the other isotopic species can be used, but the optogalvanic effect was largest for the highest gain laser lines. The transitions used in these studies are the P(22) $^{12}CO_2$ line at 10.6 μm for ^{12}C detection and the corresponding $^{13}CO_2$ line at 11.2 μm for ^{13}C. These lines are automatically in resonance with the same molecular transitions in the sample and are the highest gain and power transitions in the laser used.

The sample is maintained in a low-power (1- to 5-W) rf gas discharge, which maintains a large population of excited states in equilibrium. The optogalvanic effect is the result of a change in the effective electrical impedance of the gas discharge, which is caused by an optically induced change in the electron energy distribution function. This change results from a modification in the ionization rate that is attributable to the resonant-laser–induced change in molecular excited-state populations.

A typical response to a $^{13}CO_2$ resonance in natural CO_2 (about 1% $^{13}CO_2$) is shown in Fig. 2. The laser was modulated at 79 Hz, and the change in average rf voltage from the oscillator maintaining the discharge was digitally averaged. The time-integrated response (lock-in average) is linear in both $^{13}CO_2$ density and applied laser power. The discharge in this case consists of about 5% CO_2 in nitrogen. A mixture of CO_2 in nitrogen greatly enhances the optogalvanic effect because of the almost resonant exchange between electronically excited N_2 and the (00°1) upper laser level in CO_2 (*16*). This is the same reason a CO_2 laser is filled predominately with N_2 gas (*17*). The equilibrium density of the metastable nitrogen level ($A^3\Sigma_u^+$) is effectively changed by stimulated emission in CO_2: The incident CO_2 laser line radiatively removes about 6.7 eV of excitation energy from the system for each interacting photon.

The change in ionization rate leads to a detected change in discharge impedance. The discharge is part of a tuned circuit, and the output rf voltage is especially sensitive to impedance changes (*12*). The signal *S*, the change in rf voltage caused by the optogalvanic effect, can be expressed as

$$S = nLI_rA\,\sigma C$$

where *n* is the number density of CO_2 molecules interacting with the laser, *L* is the length of the interaction region, I_r is the resonant laser intensity, *A* is the cross-sectional area of the laser beam, σ is the

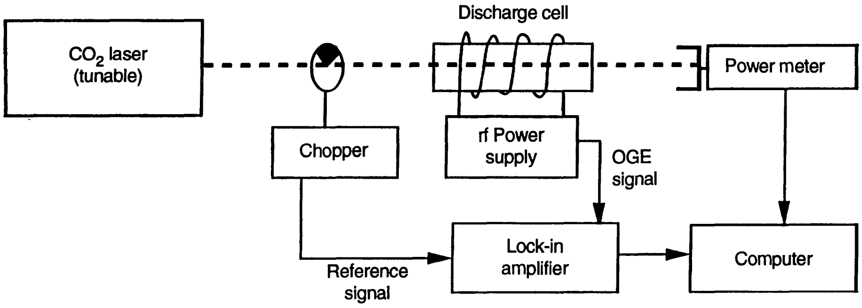

Fig. 1. Schematic diagram of laser-based carbon isotope ratio analyzer. The CO_2 laser is a grating tunable mixed isotope laser. The rf discharge circuit provides power to the discharge and monitors discharge impedance. The lock-in amplifier averages changes to the average rf voltage across the discharge in phase with the chopped laser beam. Signals are further averaged and normalized to laser power in the computer. OGE, optogalvanic effect.

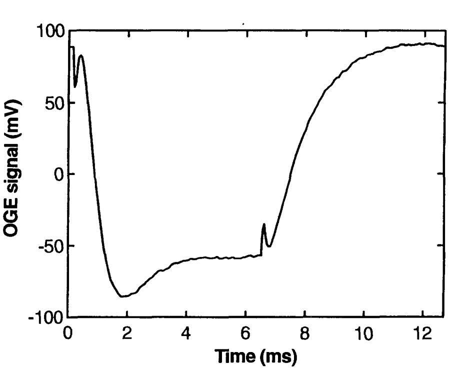

Fig. 2. The $^{13}CO_2$ response to laser at 11.2-μm resonance. The sample was desiccated exhaled normal breath. The signal was amplified by 100 with a low-noise amplifier and averaged for 10 s by digital averaging. The two small, sharp pulses indicate when the laser was turned on and turned off.

stimulated emission cross section, and C, which can be positive or negative, is an optogalvanic proportionality factor whose value depends on the detailed physics of the discharge. The constant C is a complicated function of discharge conditions, collision and ionization rates, and geometry. It cannot be accurately calculated from first principles but should be essentially independent of mass number.

When I_r is from a $^{13}CO_2$ laser line, the signal is proportional to the number density of ^{13}C. When I_r is from a $^{12}CO_2$ line, the signal is proportional to the number density of ^{12}C. The electrical signal is also linear in applied laser power for I_r below the saturation intensity $I_{sat} = h\nu/\sigma T$, where h is Planck's constant, ν is the photon frequency, and T is the relaxation time. In the discharges of interest, I_{sat} was experimentally determined to be ~3000 W/cm^2.

The isotopic ratio $^{13}CO_2:{}^{12}CO_2$ is then given by $^{13}S\ I_{12}\sigma_{12}/{}^{12}S\ I_{13}\sigma_{13}$. The optogalvanic proportionality constant can be assumed to be independent of isotope or to modify slightly the effective laser interaction cross section ratio σ_{13}/σ_{12}. The theoretical value for σ_{13}/σ_{12} can be calculated (*18*) and is 1.67, thus favoring detection of the rarer isotope. In practice, to achieve the accuracy required, one must determine σ_{13}/σ_{12} experimentally using a calibrated gas mixture. The isotopic ratio of the unknown sample relative to a standard is then determined by the relative optogalvanic signals normalized to laser power. Systematic errors are minimized and measurement time decreased if the isotopic ratio of the unknown and standard samples are measured simultaneously with in-line, separated gas discharges. The actual changes in laser power in traversal of a discharge cell are almost too small to measure. A double ratio

$$\frac{^{13}S_x}{^{12}S_x}\Big/\frac{^{13}S_{std}}{^{12}S_{std}}$$

where x refers to the unknown and std to the standard samples, then yields the desired δ directly; all other parameters, including laser power, cancel out. The accuracy of the measurement is determined by the standard used, and the precision by the average electrical signal-to-noise ratios.

In our laboratory, using the P(22) transitions at 10.6114 μm for $^{12}CO_2$ and 11.1713 μm for $^{13}CO_2$, we determined isotopic ratios of normal CO_2 samples to ±0.2 δ units with 100-s averaging times. About 9 W of laser power was used for $^{13}CO_2$, yielding signals such as that shown in Fig. 2. To avoid electrical saturation in the much larger $^{12}CO_2$ signal, the laser power at the 10.6-μm line was attenuated to about 500 mW, thus demonstrating, in one set of measurements, a sensitivity to CO_2 concentration that ranges over two orders of magnitude. An order of magnitude improvement in precision can be easily achieved either with higher laser powers for the weaker $^{13}CO_2$ signal or with longer averaging times, or with both.

The minimum detectable signal is comparable to the precision of a single measurement and corresponds to $^{13}CO_2$ concentration of about one part in a million. A typical discharge volume is 5.5 ml, operated at 0.15-torr partial CO_2 pressure. The optimal sample system consists of 5% CO_2 in nitrogen. At the low-rf discharge powers used, loss of CO_2 through dissociation, for example, is slow and not isotope-selective. Therefore, a sample can be stored and reanalyzed at any time. Conceivably, dilute impurities could influence the measurement through accidental coincidences (*19*) of laser lines with infrared resonance transitions in the impurity. Such laser resonances, however, are unlikely also to have an amplified optogalvanic effect in nitrogen.

Two calibration samples were tested relative to laboratory-bottled CO_2: one depleted in $^{13}CO_2$ (99.95% $^{12}CO_2$) (*20*) and the second near natural abundance (1.0675% $^{13}CO_2$) (*21*). The results, δ = −984.96 and δ = −62.37, respectively, imply that the laboratory gas was slightly enriched in $^{13}CO_2$, δ_{PDB} = 22.6 (*6*), and the abundance of the $^{12}CO_2$-enriched sample was actually 99.98%. Subsequent measurements with a mass spectrometer confirmed that the latter sample was indeed 99.98% $^{12}CO_2$.

As an example of the use of the technique for medical diagnostics and to demonstrate sensitivity to small changes in normal isotopic ratios, we measured the change in the $^{13}CO_2:{}^{12}CO_2$ ratio of exhaled breath as a function of time after the ingestion of 100 mg of $NaH^{13}CO_3$ by a normal subject (Fig. 3). The time response and magnitudes of the isotopic ratio changes were similar to those reported in mass spectroscopic studies of bicarbonate kinetics (*22*). The only sample preparation was that the subject's breath was passed through a dessicator before it entered the discharge cell. The presence of oxygen in the CO_2-N_2 mixture reduces the optogalvanic effect 30 to 50% compared with the optimal $CO_2(5\%)$-$N_2(95\%)$ mixture, but it has no effect on the isotope ratio result.

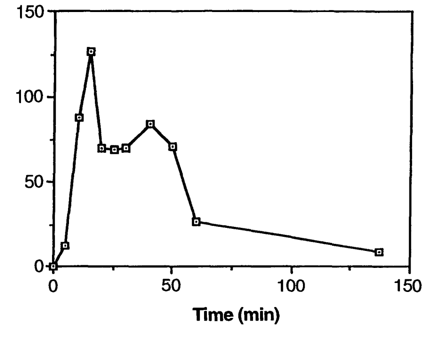

Fig. 3. Change in $^{13}CO_2$ in breath following ingestion of a 100-mg $NaH^{13}CO_3$ tablet. All measurements are referenced to breath at time 0.

Our technique favorably compares with the more complex isotope ratio mass spectrometer method. Extension of this technique to isotopic ratios for the stable oxygen isotopes ^{18}O and ^{17}O is straightforward. The techniques described should also be useful for other species for which a suitable laser transition and optogalvanic effect can be found.

REFERENCES AND NOTES

1. J. Quade and T. E. Cerling, *Science* **250**, 1549 (1990).
2. P. D. Quay, B. Tilbrook, C. S. Wong, *ibid.* **256**, 74 (1992).
3. T. E. Chapman, R. Berger, D. J. Reijngoud, A. Okken, Eds., *Stable Isotopes in Paediatric Nutritional and Metabolic Research* (Intercept Ltd., Andover, United Kingdom, 1991).
4. D. Graham *et al.*, *Lancet* i, 1174 (1987).
5. P. Krumbiegel, *Stable Isotope Pharmaceuticals For Clinical Research and Diagnosis* (Fischer, Jena, Germany, 1991).
6. Typically, isotopic ratios are quoted in δ units, where δ is the difference between an unknown and a standard in parts per thousand.

$$\delta = \left(\frac{IR_x}{IR_{std}} - 1\right) \times 1000$$

where IR_{std} = 0.011237 is the isotopic ratio for the standard Pee Dee belemnite dolomite carbon. In most studies, δ is ±1 to ±50, but an accuracy of 0.1 is important in some cases.
7. D. E. Nelson, *Science* **251**, 552 (1991).
8. P. Planarosa, Y. Demers, J. M. Gagne, *J. Opt. Soc. Am. B* 1, 704 (1984).
9. W. H. King, *Isotope Shifts in Atomic Spectra* (Plenum, New York, 1984).
10. P. S. Lee and R. F. Majkowski, *Appl. Phys. Lett.* **48**, 619 (1986).
11. B. Barbieri, N. Beverini, A. Sasso, *Rev. Mod. Phys.* **62**, 603 (1990); R. S. Stewart and J. E. Lawler, Eds., *Optogalvanic Spectroscopy 1990*, vol. 113 of the Institute of Physics (IOP) Conference Series (IOP Publishing, Bristol, United Kingdom, 1991).
12. R. D. May and P. H. May, *Rev. Sci. Instrum.* **57**, 2242 (1986).
13. Our sealed laser was manufactured by Laser Ultratech, Ontario, Canada.
14. W. W. Duley, *CO_2 Lasers Effects and Applications* (Academic Press, New York, 1976).
15. L. C. Bradley, K. L. Soohoo, C. Freed. *IEEE J. Quantum Electron.* **22**, 234 (1986).
16. W. Chaohua and Y. Mingjlang, *Chin. Phys. Lett.* **3**, 501 (1986).
17. C. K. N. Patel, *Phys. Rev. Lett.* **13**, 617 (1964).
18. M. Silver, T. S. Hartwick, M. J. Posakony, *J. Appl. Phys.* **41**, 4566 (1970).
19. R. E. Muenchausen, R D. May, G. W. Hills, *Opt. Commun.* **48**, 317 (1984).
20. Purchased from Cambridge Isotope Laboratories, Woburn, MA, and subsequently measured at Geochron Laboratories, Cambridge, MA.
21. Purchased from Oztech Corp., Dallas, TX, and measured at Southern Methodist University Stable Isotope Laboratory.
22. The detection of $^{13}CO_2$ in the breath from metabolism of labeled $NaHCO_3$ is frequently used to calibrate $^{13}CO_2$ breath tests; T. Keles, H. Paust, G. Knoblach, W. Park, in (*3*), pp. 279–287.
23. Supported by the National Institutes of Health (RO3 RR06976-01) and Rutgers University. We acknowledge C. Freed and A. Crane for discussions, D. Yeboah-Amankwah for participating in some of the early experiments, and M. Colgan for providing crucial assistance in data analysis. B.J.P. was an undergraduate research participant.

12 August 1993; accepted 10 January 1994